

Spectral absorption-based estimates of phytoplankton community composition in the North Atlantic Ocean

Alison Chase^{1*}, Emmanuel Boss¹, Lee Karp-Boss¹, Nils Haëntjens¹, Mimi Edmondson¹, Jason Graff², Michael Behrenfeld²

¹School of Marine Sciences, University of Maine, Orono, ME USA

²Department of Botany & Plant Pathology, Oregon State University, Corvallis, OR USA

*contact: alison.p.chase@maine.edu

Introduction & Background

Phytoplankton growth and biomass in the North Atlantic Ocean is highly dynamic in time and space (Barton et al., 2015; Sabine et al., 2004), but for ocean basin-scale observations, chlorophyll *a* (Chl *a*) estimated from satellite is the only currently available approach. A measure of total Chl *a* or phytoplankton biomass alone tells us little about the composition of phytoplankton in the water and hence about the structure and functioning of the ecosystem. Morphological, genomics, chemical (e.g. pigments) and optical methods have been used in various studies to assess phytoplankton community composition. Of these, optical methods offer potential significance in enhancing the spatial and temporal coverage at which changes in phytoplankton composition can be monitored. Optical measurements, made both by satellite and with instruments deployed on ships that operate continuously, provide data at a higher spatial and temporal resolution than discrete water samples. Previous studies using multispectral optical data to detect phytoplankton community composition (specifically diatoms) have met with challenges during attempts to validate them independently (Kramer et al., 2018). Hyperspectral optical information (i.e. absorption and reflectance spectra) is attainable using in situ instruments, and provides increased information over that available from multispectral data (Vandermeulen et al., 2017). Future satellite-borne instruments such as the Ocean Color Instrument (OCI) to be flown on NASA's PACE satellite will provide hyperspectral information from space within the coming decade; therefore, the development and evaluation of methods using hyperspectral optical measurements to address unanswered oceanographic questions is necessary in anticipation of global-scale hyperspectral information (Bracher et al., 2017).

A major challenge in the detection of shifts in the phytoplankton community is the general co-variation of Chl *a* and all phytoplankton accessory pigments in the ocean (Trees et al., 2000). Methods such as CHEMTAX (Mackey et al., 1996) have exploited the variability of accessory pigments relative to Chl *a* to gain insight into phytoplankton community composition given known pigment ratio values for different phytoplankton groups. Although there is high variability in pigment ratios due to environmental growth conditions including light and nutrient availability (Roy et al., 2011), previous studies have shown success in the use of variable ratio values to identify major phytoplankton community shifts (e.g. Swan et al., 2016). In this study, we exploit the information contained in hyperspectral absorption measurements to estimate phytoplankton accessory pigment concentrations and their values relative to Chl *a*; these ratios are then used as indicators of community composition. We use imaging flow cytometry as an independent

analysis of the phytoplankton community, and highlight times and places during different seasons when Chl *a* information alone would provide an incomplete picture regarding phytoplankton community composition.

Approach

The objective of this study is to evaluate the use of optically-derived accessory pigments, namely total chlorophyll *b* and chlorophyll c_1+c_2 (denoted Chl *b* and Chl *c* for the remainder of this paper, respectively), and their ratios to Chl *a* as indicators of phytoplankton community composition. In particular, we aim to understand whether the knowledge of these pigments can provide information beyond what would be estimated given only knowledge of Chl *a* (e.g. bulk phytoplankton biomass).

Data for this analysis were collected during two different research cruises of the North Atlantic Aerosol and Marine Ecosystems Study (NAAMES) investigation on the R/V Atlantis: one in late spring (NAAMES 02, May 2016), and one in late summer (NAAMES 03, September 2017; Figs. 1-2). Data from two additional cruises (NAAMES 01 and 04, November 2015 and April 2018, respectively) are still being processed and will be added during future analyses. An ac-s spectral absorption and attenuation sensor (Sea-Bird Scientific, Philomath, OR, USA) and Imaging FlowCytobot (IFCB, McLane Research Laboratories, Inc., East Falmouth, MA, USA) were both deployed in an in-line configuration allowing for continuous sampling of surface waters (~5 meters) along the ship track (note that mixing depth was always below the depth of the water intake). For phytoplankton pigment analysis, discrete seawater samples were collected from the flowing seawater source of the ship and filtered onto 25 mm GF/F filters, and immediately store in liquid nitrogen. Filters were analyzed for phytoplankton pigment concentrations using High Performance Liquid Chromatography (HPLC) analysis at the Ocean Ecology Laboratory at NASA Goddard Space Flight Center, following methods in Van Heukelem and Thomas (2001) and Hooker et al. (2009).

Particulate absorption spectra ($a_p(\lambda)$; λ denotes wavelength in nm) were calculated using a calibration-independent method made possible by the diversion of seawater in the in-line system through a 0.2 μm filter for 10 minutes every hour (Slade et al., 2010). The $a_p(\lambda)$ spectra were binned to a one-minute resolution and data were analyzed manually to remove any periods of bubbles in the water or other known problems. A total of 21,649 and 18,539 spectra were collected during NAAMES 02 and NAAMES 03, respectively, and are used in the present study. Estimation of phytoplankton pigments from $a_p(\lambda)$ spectra was completed following methods in Chase et al. (2013). Briefly, the $a_p(\lambda)$ spectra were decomposed into a series of Gaussian functions, and the magnitude of individual Gaussian peak absorption ($a_{\text{gaus}}(\lambda)$) is used to estimate the concentrations of Chl *a*, Chl *b* and Chl *c* from absorption at 675 nm, 660 nm, and 638 nm, respectively:

$$\text{Chl } a = \left(\frac{a_{\text{gaus}}(675 \text{ nm})}{0.020} \right)^{\frac{1}{0.96}} \quad (1)$$

$$Chl\ b = \left(\frac{a_{gaus}(660\ nm)}{0.018} \right)^{\frac{1}{0.87}} \quad (2)$$

$$Chl\ c = \left(\frac{a_{gaus}(638\ nm)}{0.031} \right)^{\frac{1}{0.86}} \quad (3)$$

The coefficients used in Eq. (1-3) were determined by re-tuning the Chase et al. (2013) algorithm to the North Atlantic region addressed in the present study by comparing $a_{gaus}(\lambda)$ magnitudes and HPLC pigment information collected during the NAAMES 02 and 03 campaigns, as well as during NAAMES 01 (November 2015). The median error values for the estimation of Chl *a*, Chl *b*, and Chl *c* using the Eq. (1-3) are 9%, 34%, and 18%, respectively.

For morphological and taxonomic analysis of phytoplankton community composition, 5 ml samples of seawater from the flow-through system were imaged based on a laser-induced chlorophyll fluorescence threshold with the IFCB at a sampling frequency of 1 sample per 20 minutes. Images and associated metadata were then uploaded to the EcoTaxa server for taxonomic identification and classification (<http://ecotaxa.obs-vlfr.fr/>; Picheral et al., 2017). A random forest classification algorithm was used for the prediction of the taxonomic identification of each image, and a set of manually classified images from the North Atlantic Ocean was used to train the algorithm and followed by manual image validation.

To compare phytoplankton pigments derived from $a_p(\lambda)$ and IFCB imagery data, median values of pigment data from within +/- 15 minutes of a given IFCB sample date/time were used. IFCB data were exported from EcoTaxa and processed to combine images into one of 9 categories: Chlorophyta, Cryptophyta, diatoms, dinoflagellates, Euglenophyta, Prymnesiophyceae, silicoflagellates, unidentifiable, and non-living. The silicoflagellates (namely Dictyochales), Prymnesiophyceae, and Cryptophyta are combined into one group to represent the Chl *c*-containing phytoplankton that are present in addition to diatoms and dinoflagellates (Jeffrey and Vesk, 1997). Chlorophyta (includes Prasinophytes) and Euglenophyta are combined to represent Chl *b*-containing phytoplankton (Jeffrey and Vesk, 1997). Due to known underestimation by the IFCB of particles <8 μm , only particles >8 μm are included in the analysis. Across all data presented here, unidentifiable cells are dominated by nanoplankton, as ~95% of all unidentifiable cells have an equivalent spherical diameter between 8-20 μm . The non-living category includes detritus and fecal pellets. Images identified as bubbles, beads (present as residual from IFCB instrument calibration), and images that are out of focus and therefore not identifiable as living or non-living are removed during processing. Ciliates and Rhizaria are also identified but comprise < 2% of all data (in units of $\mu\text{m}^2\ \text{ml}^{-1}$) and are not included in the present analysis.

To date, community composition derived from IFCB data has been obtained at 30 and 49 locations along the cruise track for NAAMES 02 (May) and NAAMES 03 (September), respectively. For a given location, the IFCB files within +/- 3 hours of discrete water

sample collection for HPLC pigment analysis are identified while also checking to see that all files have a median equivalent spherical diameter value within 20% of the closest matching file in time. The taxonomic validation of images is then completed for all matching files in the 6-hour span (maximum of 15 files) or until ~3,000 images have been validated; for example, in some cases the closest matching two files may have >3,000 images and are thus sufficient to represent the phytoplankton community, and in other cases all 15 files from the 6-hour span are used in an effort to increase the number of images and more accurately represent community composition.

Results

The NAAMES 02 cruise took place May 11 – June 5, 2016 during which time the ship passed through several areas with relatively high ($>2 \text{ mg m}^{-3}$) regions of Chl *a* concentration as well as several distinct water masses as seen in surface temperature information (Fig. 1A-B). Chl *a* concentrations are approximately log-normally distributed, spanning approximately $0.5\text{--}5 \text{ mg m}^{-3}$ and with a median value of 1.2 mg m^{-3} . There are several regions of the study area where the phytoplankton community composition can be explained by relative changes in the optically-derived pigments and pigment ratios (Fig. 2; Table 1). During the time period from May 19 – May 21 Chl *a* was relatively constant at around 3 mg m^{-3} ; however, the phytoplankton community shifted first to a nanoplankton and dinoflagellate-dominated regime, which was followed by an increase in diatoms. An increase in relative Chl *b* and Chl *c* on May 29 is clear in the accessory pigment ratio values coincident with a peak in Chl *a* concentration; in this case again the presence of high relative accessory pigments indicates a nanoplankton and dinoflagellate (i.e. non-diatom) dominated phytoplankton community.

The NAAMES 03 cruise provides information on a different part of the annual phytoplankton cycle; in contrast to the relatively high Chl *a* concentrations observed during NAAMES 02, NAAMES 03 took place Aug 30 – Sept 24, 2017. Chl *a* concentrations are distributed around a median value of $\sim 0.4 \text{ mg m}^{-3}$, and spanning approximately $0.1\text{--}1 \text{ mg m}^{-3}$. However, several distinct water masses were sampled and the environmental variability is apparent in Fig 3A-B. The most prominent feature in the pigment and phytoplankton composition data is the time period when the ship was at its northernmost point, during approximately September 13 – 18 (Fig 4). Chl *a* concentration increases rapidly from $<0.5 \text{ mg m}^{-3}$ to $\sim 1 \text{ mg m}^{-3}$, where it remains for the duration of the six days. Chl *b*:Chl *a* also exhibits a similar increase, while Chl *c*:Chl *a* remains essentially unchanged relative to before and after this time. The phytoplankton community composition during this time shows a small increase in diatoms, and a much more notable increase in the particle area of both nanoplankton and dinoflagellates (Fig. 4). A second notable feature in the pigment and composition data is a prominent diatom peak observed on September 21, along with a clear corresponding increase in Chl *a* concentration while the accessory pigment ratios remain constant during this time.

Discussion & Conclusions

The positive correlation between Chl *a* and the total area of all phytoplankton $>8 \mu\text{m}$ ($r^2 = 0.89$; Fig 5) precludes the use of Chl *a* alone to predict phytoplankton community composition. However, the additional information provided by the relative concentrations of Chl *b* and Chl *c* gives insight into the phytoplankton community present at a given location. In addition, the variability of accessory pigment ratios can be used to identify a shift in community composition that would otherwise go unnoticed given relatively constant Chl *a* concentration. Extension of the work presented here to hyperspectral $R_{rs}(\lambda)$ data is possible via previous work showing that accessory pigments can also be estimated from $R_{rs}(\lambda)$ using an inversion that incorporates the Gaussian decomposition method (Chase et al., 2017). The Chase et al. (2017) study also shows that pigments cannot be estimated more accurately from $R_{rs}(\lambda)$ than they can from pigment co-variation. However, even if predictive errors are similar, the Gaussian method of pigment estimation results in accessory pigment information independent from Chl *a*, and the work presented here shows that this is necessary for enhanced analysis of phytoplankton community composition.

The major findings of this study are as follows:

1. Increased values of Chl *b*:Chl *a* and Chl *c*:Chl *a* can be used to indicate that a coincident increase in Chl *a* concentration is due to a non-diatom dominated phytoplankton community.
2. Periods of relatively constant Chl *a* but changing phytoplankton community composition can be detected by increased Chl *b*:Chl *a* and/or Chl *c*:Chl *a*.

These findings highlight a path forward regarding a key goal within optical oceanography: to observe large-scale phytoplankton community composition patterns. This knowledge will enable studies that address what drives these community composition patterns (e.g. water mass history, environmental conditions, mixing, etc.). Future work will expand on our present analysis to include increased coverage of phytoplankton community composition from imagery data, allowing for development of a robust relationship between the composition and accessory pigments ratios intended for application with future satellite-based hyperspectral reflectance measurements. The work presented here demonstrates both the need for moving beyond Chl *a*-based algorithms to detect changes in the phytoplankton community, and the ability of optically-estimated accessory pigment concentrations to address this need.

References

- Barton, A. D., M. S. Lozier, R. G. Williams, Physical Controls of Variability in North Atlantic Phytoplankton Communities. *Limnol. Oceanog.* **60** (1), 181–97 (2015).
- Bracher, A., H. Bouman, R. J. Brewin, A. Bricaud, A. M. Ciotti, L. Clementson, E. Devred, et al., Obtaining Phytoplankton Diversity from Ocean Color: A Scientific Roadmap for Future Development. *Frontiers in Marine Science* **4** (March), 1–15 (2017).
- Chase, A., E. Boss, R. Zaneveld, A. Bricaud, H. Claustre, J. Ras, T. K. Westberry, Decomposition of in situ particulate absorption spectra. *Methods in Oceanography* **7**, 110–124 (2013).
- Chase, A., E. Boss, I. Cetinić, W. Slade, Estimation of Phytoplankton Accessory Pigments from Hyperspectral Reflectance Spectra: Toward a Global Algorithm. *Journal of Geophysical Research: Oceans* **122** (2017).
- Hooker, S. B., L. V. Heukelem, C. S. Thomas, H. Claustre, J. Ras, L. Schluter, J. Perl, The Third SeaWiFS HPLC analysis round-robin experiment (SeaHARRE- 3). Goddard, MD: National Aeronautics and Space Administrations. (2009).
- Jeffrey, S. W., M. Vesk, Introduction to marine phytoplankton and their pigment signatures, in: Phytoplankton pigment in oceanography: Guidelines to modern methods. Edited by: Jeffrey, S. W., R. F. C. Mantoura, S. W. Wright, UNESCO, 33–84 (1997).
- Kramer, S. J., C. S. Roesler, H. M. Sosik, Bio-optical discrimination of diatoms from other phytoplankton in the surface ocean: Evaluation and refinement of a model for the Northwest Atlantic. *Remote Sensing of Environment* **217**, 126-143 (2018).
- Mackey, M. D., D. J. Mackey, H. W. Higgins, S. W. Wright, CHEMTAX- a Program for Estimating Class Abundances from Chemical Markers: Application to HPLC Measurements of Phytoplankton. *Mar. Ecol. Progr. Ser.* **144**, 265–83 (1996).
- Picheral M., S. Colin J-O., Irisson, EcoTaxa, a tool for the taxonomic classification of images. <http://ecotaxa.obs-vlfr.fr>. (2017).
- Roy, S., E. S. Egeland, C. Llewellyn, G. Johnsen, Phytoplankton Pigments: Characterization, Chemotaxonomy and Applications in Oceanography. Cambridge University Press (2011).
- Sabine, C. L., R. A. Feely, N. Gruber, R. M. Key, K. Lee, J. L. Bullister, R. Wanninkhof, et al., The Oceanic Sink for Anthropogenic CO₂. *Science* **305** (5682), 367–71 (2004).
- Slade, W. H., E. Boss, G. Dall’olmo, M. R. Langner, J. Loftin, M. J. Behrenfeld, T. K. Westberry, Underway and moored methods for improving accuracy in measurement of

spectral particulate absorption and attenuation. *Journal of Atmospheric and Oceanic Technology* **27** (10), 1733–1746 (2010).

Swan, C. M., M. Vogt, N. Gruber, C. Laufkoetter, A Global Seasonal Surface Ocean Climatology of Phytoplankton Types Based on CHEMTAX Analysis of HPLC Pigments. *Deep-Sea Research Part I: Oceanographic Research Papers* **109** 137–56 (2016).

Trees, C. C., D. K. Clark, R. R. Bidigare, M. E. Ondrusek, J. L. Mueller, Accessory pigments versus chlorophyll a concentrations within the euphotic zone: A ubiquitous relationship. *Limnology and Oceanography* **45** (5), 1130–1143 (2000).

Van Heukelem, L., C. S. Thomas, Computer-assisted high-performance liquid chromatography method development with applications to the isolation and analysis of phytoplankton pigments. *Journal of Chromatography A* **910**, 31–49 (2001).

Vandermeulen, R. A., A. Mannino, A. R. Neeley, P. J. Werdell, R. Arnone, Determining the Optimal Spectral Sampling Frequency and Uncertainty Thresholds for Hyperspectral Remote Sensing of Ocean Color. *Optics Express* **25** (16), 785–97 (2017).

Figures & Table

Table 1. Time periods of increased (arrows) or neutral (horizontal lines) pigment concentrations (units of Chl *a* are mg m⁻³) or pigment ratios (ratios are unitless) during the NAAMES 02 (May 2016) and NAAMES 03 (September 2017) cruises. Community composition column indicates the dominant phytoplankton community (in terms of particle area, units of μm² ml⁻¹) and determined using IFCB imagery data.

Date(s)	Chl <i>a</i>	Chl <i>b</i> :Chl <i>a</i>	Chl <i>c</i> :Chl <i>a</i>	Community composition
May 19-21	—	↑	—	nanoplankton
May 29	↑	↑	↑	nanoplankton & dinoflagellates
September 13-18	↑	↑	—	nanoplankton & dinoflagellates
September 21	↑	—	—	diatoms

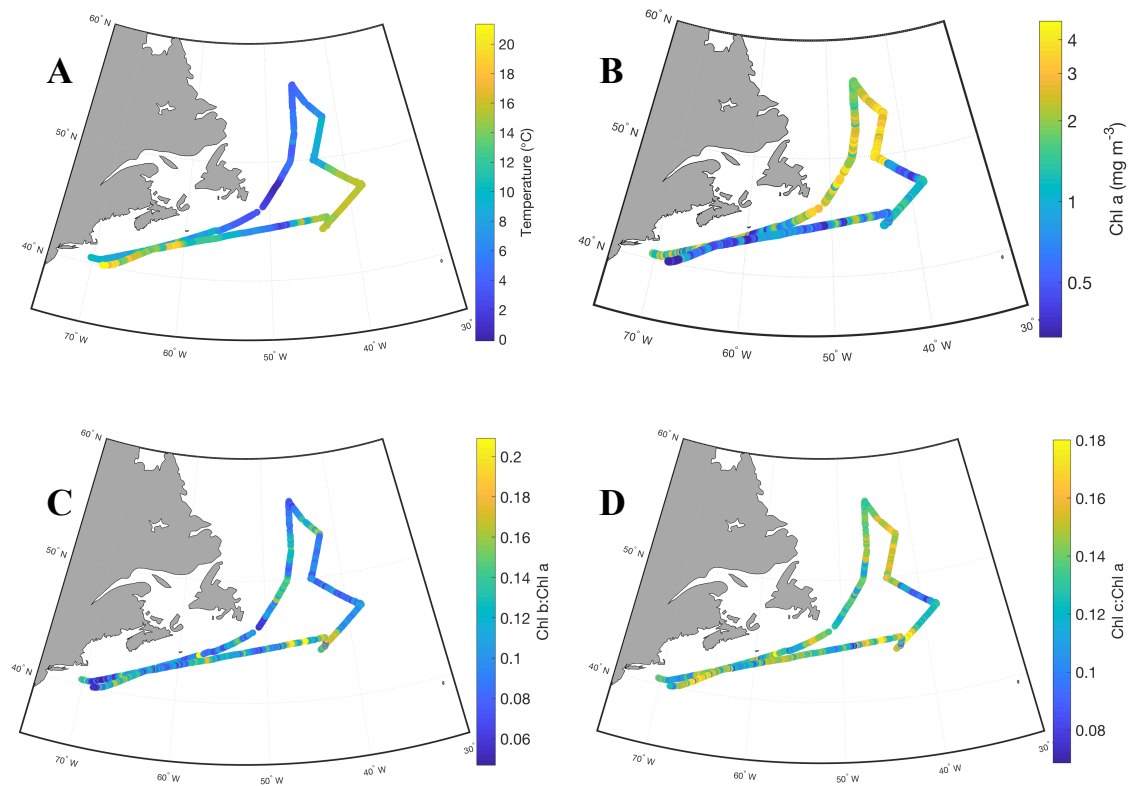


Figure 1. NAAMES 02 (May 2016) ship track (clockwise) and (A) surface water temperature (deg C), (B) Chl *a* (mg m⁻³), (C) Chl *b*:Chl *a*, and (D) Chl *c*:Chl *a*. Pigments are derived from in situ hyperspectral absorption measurements following a re-tuned version of the methods in Chase et al. (2013) and represent surface waters (~5 m depth). Total n = 21,649.

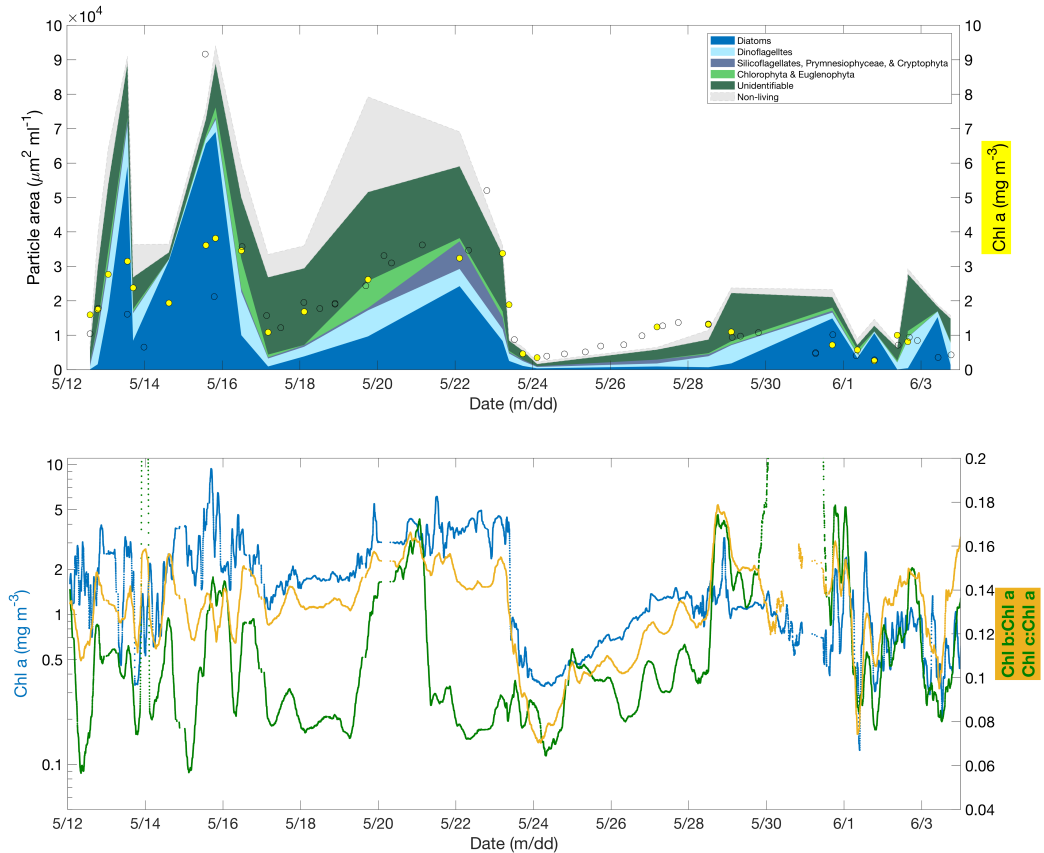


Figure 2. Top panel: particle area (left y-axis, $\mu\text{m}^2 \text{ml}^{-1}$) by phytoplankton group through time during NAAMES 02 (diatoms, dinoflagellates, summed silicoflagellates + Prymnesiophytes + Cryptophytes, summed Chlorophyta + Euglenophyta, and unidentifiable nanoplankton), as well as non-living particles shown in light gray. Chlorophyll *a* concentrations (right y-axis, mg m^{-3}) from HPLC analysis show all available data, and dates with matching IFCB imagery data shown in the area plot are filled yellow circles. Bottom panel: Chl *a* (blue line, mg m^{-3} , left y-axis), Chl *b*:Chl *a* (green line) and Chl *c*:Chl *a* (yellow line; both unitless right y-axis) shown through time (matching the timespan of the top panel).

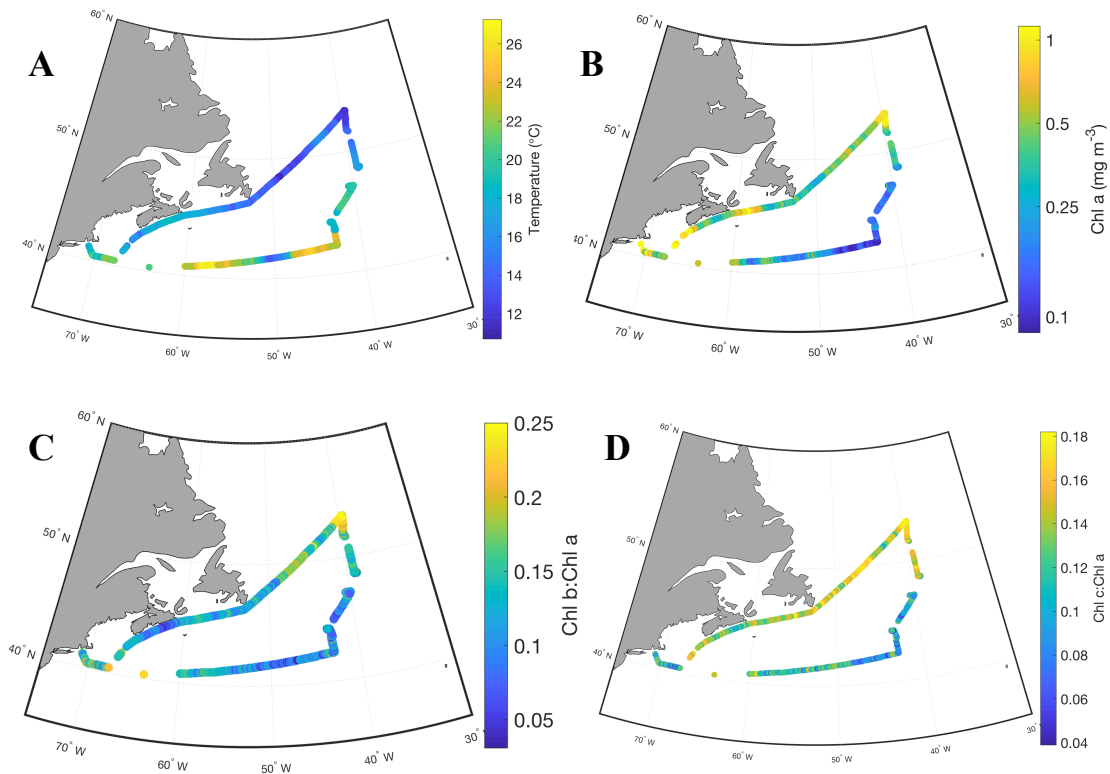


Figure 3. NAAMES 03 (September 2017) ship track (counter-clockwise) and (A) surface water temperature (deg C), (B) Chl *a* (mg m^{-3}), (C) Chl *b*:Chl *a*, and (D) Chl *c*:Chl *a*. Pigments are derived from in situ hyperspectral absorption measurements following a re-tuned version of the methods in Chase et al. (2013) and represent surface waters (~ 5 m depth). Total $n = 18,539$.

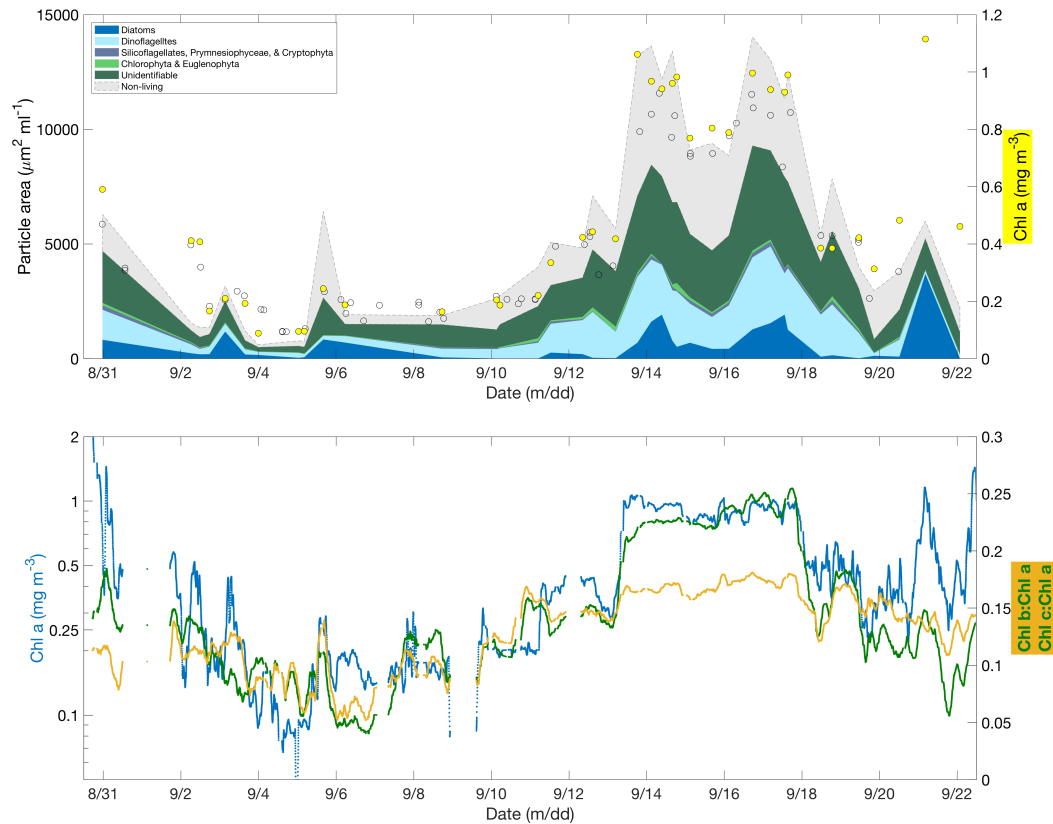


Figure 4. Top panel: particle area (left y-axis, $\mu\text{m}^2 \text{ml}^{-1}$) by phytoplankton group through time during NAAMES 03 (diatoms, dinoflagellates, summed silicoflagellates + Prymnesiophytes + Cryptophytes, summed Chlorophyta + Euglenophyta, and unidentifiable nanoplankton), as well as non-living particles shown in light gray. Chlorophyll *a* concentrations (right y-axis, mg m^{-3}) from HPLC analysis show all available data, and dates with matching IFCB imagery data shown in the area plot are filled yellow circles. Bottom panel: Chl *a* (blue line, mg m^{-3} , left y-axis), Chl *b*:Chl *a* (green line) and Chl *c*:Chl *a* (yellow line; both unitless right y-axis) shown through time (matching the timespan of the top panel).

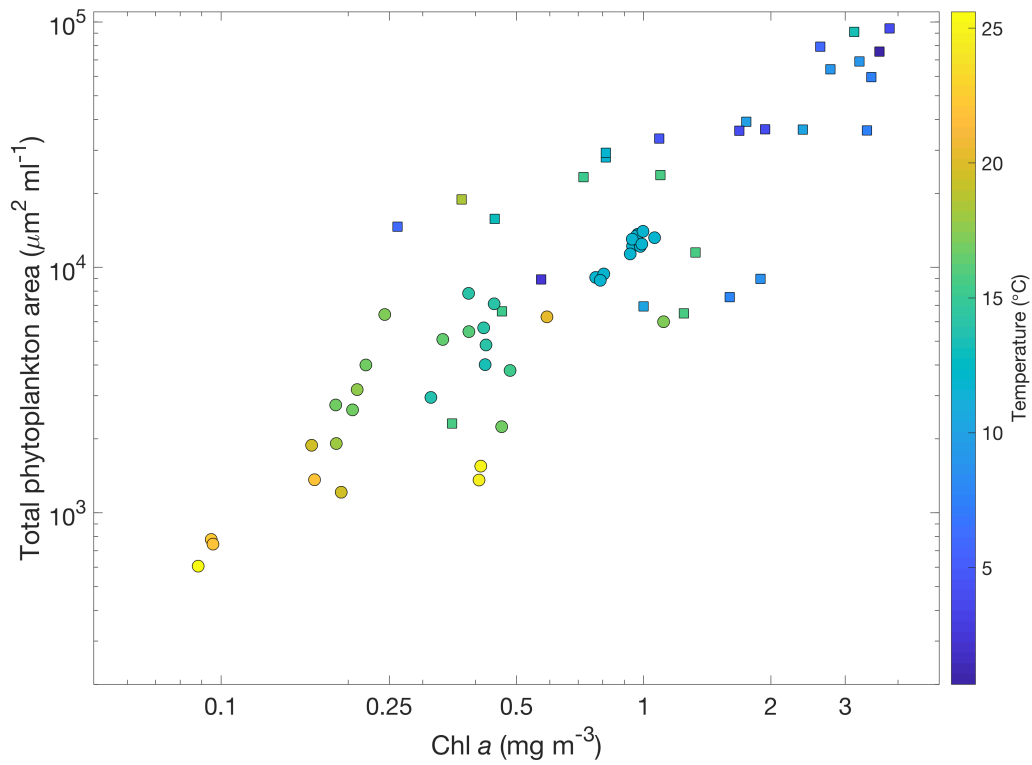


Figure 5. Chlorophyll *a* estimated from absorption spectra versus the area of all living particles analyzed with the IFCB; both data sets represent surface water (~ 5 m). The color of the points indicates surface water temperature (deg C) at the time of sample collection. Total number of points is 79: there are 30 from NAAMES 02 (May 2016) and 49 from NAAMES 03 (September 2017). Correlation coefficient for all 79 points is $r^2 = 0.89$.